IEEE Access
Multidisciplinary | Rapid Review | Open Access Journal

Received May 18, 2018, accepted July 11, 2018, date of publication July 20, 2018, date of current version August 15, 2018.

Digital Object Identifier 10.1109/ACCESS.2018.2857006

Dual-View Display Based on Spatial Psychovisual Modulation

ZHONGPAI GAO AND GUANGTAO ZHAI, (Member, IEEE)
Institute of Image Communication and Information Processing, Shanghai Jiao Tong University, Shanghai 200240, China

Corresponding author: Guangtao Zhai (zhaiguangtao@sjtu.edu.cn)

This work was supported in part by NSFC under Grant 61331014 and Grant 61521062 and in part by the Equipment Pre-Research Joint Research Program of Ministry Education under Grant 6141A020223.

ABSTRACT Dual-view display is a technology that provides two different views concurrently for different users on a single medium. We propose a dual-view display system, where users can see one view through a pair of specific glasses (called *personal view*) and see another view without the glasses (called *shared view*). The display technology can be of great use in practice. For instance, in the application of information security display, the user with the specific glasses can see the private information but bystanders can only see an unrelated/disguising view. The dual-view display is based on an information display technology called spatial psychovisual modulation (SPVM). The rationale behind SPVM is that modern displays have high resolutions and can provide information beyond what human visual system can resolve, i.e., modern displays have spatial psychovisual redundancy. The redundancy of high-resolution displays can be exploited to achieve dual-view or even multi-view display. In this paper, we introduce heuristic and iterative algorithms for the dual-view display. The iterative algorithm utilizes the Gaussian-like spatial integration window of human eyes. Compared with the heuristic algorithm, the iterative algorithm has significant improvements for the *shared view* with preference in percentage of 90.2% on average. This paper serves as a guidance for dual-view-based applications. Moreover, the method discussed in this paper can be also used to explore the temporal redundancy of displays.

INDEX TERMS Display technology, dual-view, signal processing, spatial psychovisual modulation.

I. INTRODUCTION

Dual-view display aims to present two different images simultaneously on a single medium. The most proven technology used for dual-view display is the existing stereoscopic 3D (S3D) techniques [1] that provide two views for the left and right eyes, respectively. In S3D displays, four types of methods are generally used to separate the left and right views in a single screen: temporal multiplexing (shutter glasses), spatial multiplexing (polarization), color multiplexing (anaglyph), and angular multiplexing (autostereoscopic). Instead of two views for the left and right eyes, S3D techniques can be used to provide two different views for two different users where each user's both eyes see the same view. For the temporal multiplexing [2], [3], spatial multiplexing, and color multiplexing methods, users can see two different views using two different pairs of glasses. The left and right sides of each pair of the glasses use the same filter. For the angular multiplexing method [4], two viewers from different viewing angles can see two different images and additional optical elements (e.g., glasses) are not needed [5], [6].

The deficiency of the dual-view display using these multiplexing methods is that the image quality deteriorates when crosstalk between the two views occurs. For temporal, spatial, and color multiplexing methods, the view without glasses is a superimposed image of the two views, which is usually not semantically meaningful. For the angular multiplexing method, viewing angles are small and the user needs to be at positions near the sweet-spot.

In this paper, we propose a dual-view display technology that provides two different views in a single screen: one view with glasses called *personal view* and another view without glasses called *shared view*, as shown in Fig. 1. The dual-view display can be used in several applications. For instance, in an information security display system [7], users with a pair of the specific glasses can see the secret information but bystanders without the glasses can only see masking or disguising images, which can be semantically meaningful but irrelevant to the secret information. Another example is a multiple exhibitions on a lone display (MELD) system by Zhai and Wu (2014), which supports multiuser collaborative

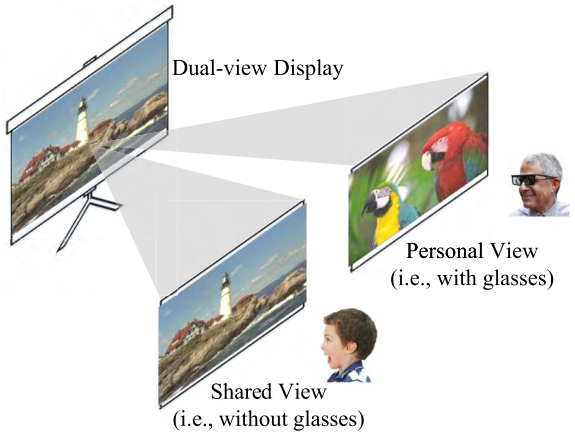

FIGURE 1. Dual-view display diagram. Two different views are presented on a single screen simultaneously. People with a pair of specific glasses see one view hidden on this screen, called *personal view* and without the glasses see another view, called *shared view*.

visualization to make the collaboration of several people efficient.

The rationale behind the proposed dual-view display technique is that: the refresh rate and resolution of modern displays are very high but the discrimination capacities of human visual systems in the spatial and temporal domain are limited. The spatial and temporal redundancies of modern displays can be explored to achieve duel-view or even multi-view display. Temporal psychovisual modulation (TPVM) [8] is a display technology utilizing the redundancy of display in the temporal domain. TPVM involves signal processing techniques, optoelectronics, and psychophysics. Human visual systems cannot detect rapidly changing luminance beyond critical fusion frequency (CFF), which is about 60 Hz in normal viewing conditions [9]. However, modern displays can reach much higher refresh rate, e.g., the binary pattern rate of digital light processing (DLP) projectors is up to 32 kHz (beyond 1900 Hz for 8-bit gray) [10]. Thus, a high refresh rate display has psychvisual redundancy in the temporal domain that can be explored to generate multiple visual percepts for different viewers simultaneously.

The idea of TPVM can be extended to the spatial domain, called spatial psychovisual modulation (SPVM). Nowadays, modern displays have high pixel density [11], e.g., Sony Xperia Z5 Premium is 801.06 pixels per inch (PPI), which is far beyond the limit that human visual systems can resolve. Human eyes without aided are difficult to differentiate detail beyond 300 PPI [12], [13]. Thus, a high pixel density display has psychovisual redundancy in spatial domain that also can be explored to generate multiple visual percepts for different viewers concurrently. In practice, polarization interlacing 3D displays (circular or linear polarization) can be used for SPVM-based dual-view display. The scan lines of the displays are divided into different polarized directions. The desired personal view can be perceived through matched polarized glasses.

In this paper, we focus on the dual-view display system that only explores the spatial psychovisual redundancy of display. Under current commercially available polarized 3D displays, several applications have been proposed and implemented based on the dual-view display technique, e.g., the information security display system introduced in [14] and the dual-view medial image visualization system proposed in [15]. In previous studies, the SPVM-based applications were computed by the heuristic algorithm that will be reviewed in Section II. Using the heuristic algorithm, the *personal view* and *shared view* are generated simply by adding or subtracting the views. Some artifacts are introduced, especially on edges. We propose a new iterative algorithm in Section III to improve the performance of the dual-view display.

TABLE 1. Basic Matrix Notations and Operations

u or U	scalar
$\mathbf{u}$	vector
$\mathbf{U}$	matrix
$\mathbf{U}_{ij}$	the entry in the i-th row and j-th column of $\mathbf{U}$
$\mathbf{U}_{i:}$	the i-th row of $\mathbf{U}$
$\mathbf{U}_{:j}$	the j-th column of $\mathbf{U}$
$\mathbf{U}^T$	the transposition of $\mathbf{U}$
$[\mathbf{U}]_{[a,b]}$	$\min\{b, \max\{a, \mathbf{U}\}\}$
$\min\{a, \mathbf{U}\}$	the entrywise minimum: $\min\{a, \mathbf{U}_{ij}\}$
$\max\{a, \mathbf{U}\}$	the entrywise maximum: $\max\{a, \mathbf{U}_{ij}\}$
$\|\mathbf{U}\|_F$	the Frobenius Norm: $\sqrt{\sum_i \sum_j \|\mathbf{U}_{ij}\|^2}$

II. HEURISTIC ALGORITHM FOR DUAL-VIEW DISPLAY

Throughout this paper, standard notations and basic matrix operations used are listed in TABLE 1. In the dual-view display system, polarized 3D displays emit two views in odd and even lines concurrently without interference. We denote the two basis images as $\mathbf{X} = [\mathbf{x}_1, \mathbf{x}_2] \in \mathbb{R}^{N\times 2}$ that are nonnegative, where $N = H \times W$ is the pixel number of each image. The *shared view* $\mathbf{y}_1$ is the addition of the two images $(\mathbf{x}_1 + \mathbf{x}_2)$ and the *personal view* $\mathbf{y}_2$ is chosen to be the odd-lines image $\mathbf{x}_1$. Thus, the weight of the *shared view* is denoted as $\mathbf{w}_1 = [1, 1]^T$ and weight of the *personal view* is $\mathbf{w}_2 = [1, 0]^T$. Therefore, the dual-view display can be formulated as

$$\begin{aligned} \mathbf{y}_1 &= \mathbf{X}\mathbf{w}_1 = \mathbf{x}_1 + \mathbf{x}_2, \\ \mathbf{y}_2 &= \mathbf{X}\mathbf{w}_2 = \mathbf{x}_1, \quad \Rightarrow \mathbf{Y} = \mathbf{X}\mathbf{W} \end{aligned} \tag{1}$$

where $\mathbf{Y} = [\mathbf{y}_1, \mathbf{y}_2] \in \mathbb{R}^{N\times 2}$, $\mathbf{W} = [\mathbf{w}_1, \mathbf{w}_2] \in \mathbb{R}^{2\times 2}$, and $\mathbf{0} \le \mathbf{X} \le \mathbf{1}$. The basis images can be computed as follows,

$$\mathbf{x}_1 = \mathbf{y}_2, \tag{2}$$

$$\mathbf{x}_2 = \mathbf{y}_1 - \mathbf{y}_2. \tag{3}$$

However, two issues need to be concerned in Equation (3):

1) Gamma correction, the correspondences between brightness and grayscale values are not linear for most screens. The calculation for the basis image $\mathbf{x}_2$ should be processed in the luminance domain.

2) Range adjustment, the basis image $\mathbf{x}_2$ may be out of the [0,1] range after the subtraction. Thus, the ranges of $\mathbf{y}_1$ and $\mathbf{y}_2$ need to be adjusted to make sure the basis image $\mathbf{x}_2$ can be presented on the screen correctly.

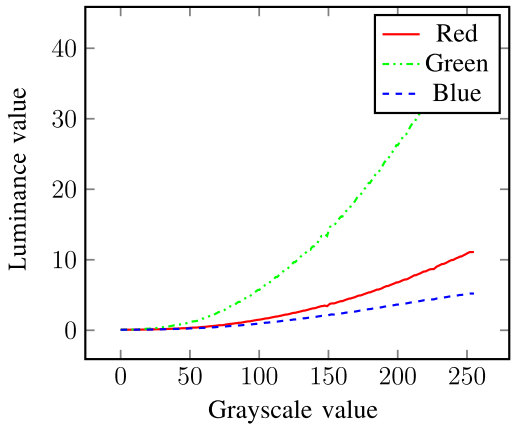

FIGURE 2. Grayscale value versus luminance value of ALIENWARE ALW17R-1948 screen measured by Konica Minolta Display Color Analyzer CA-210 [7].

Fig. 2 shows the relationship between luminance and grayscale value of an ALIENWARE ALW17R-1948 screen measured by Konica Minolta Display Color Analyzer CA-210. Based on the collected data, we can build two mapping tables *g2l* and *l2g*, which are the transformation functions from the grayscale space to the luminance space and from the luminance space to the grayscale space, respectively. Both the ranges of the grayscale space and luminance space are normalized to [0, 1]. The subtraction for $\mathbf{x}_2$ should be operated in the luminance space.

Algorithm 1 Heuristic Algorithm for Dual-View Display

Require: $\mathbf{Y} = [\mathbf{y}_1, \mathbf{y}_2] \in \mathbb{R}^{N\times 2}$, $r \in (0, 1)$
$\mathbf{l}_{y1} = g2l(\mathbf{y}_1)$; $\mathbf{l}_{y2} = g2l(\mathbf{y}_2)$;//Mapping from grayscale space to luminance space
$\mathbf{l}_{y1} \in [0, 1] \rightarrow [r, 1]$; $\mathbf{l}_{y2} \in [0, 1] \rightarrow [0, r]$;//Adjusting the luminance ranges
$\mathbf{l}_{x1} = \mathbf{l}_{y2}$; $\mathbf{l}_{x2} = \mathbf{l}_{y1} - \mathbf{l}_{y2}$; //Operations
$\mathbf{x}_1 = l2g(\mathbf{l}_{x1})$; $\mathbf{x}_2 = l2g(\mathbf{l}_{x2})$;//Mapping from luminance space back to grayscale space
return $\mathbf{X} = [\mathbf{x}_1, \mathbf{x}_2] \in \mathbb{R}^{N\times 2}$;

In luminance space, the subtraction may still result in $\mathbf{x}_2$ being out of the [0, 1] range (i.e., some elements are lower than 0 when $\mathbf{y}_1 < \mathbf{y}_2$). Thus, range adjustments in the luminance space for $\mathbf{y}_1$ and $\mathbf{y}_2$ are necessary. We set a luminance value $r \in (0, 1)$ and adjust the luminance range of $\mathbf{y}_1$ and $\mathbf{y}_2$ to $[r, 1]$ and $[0, r]$, respectively. The pseudocode of the heuristic algorithm is outlined in Algorithm 1. Because of the adjustments of luminance ranges, the *shared view* $\mathbf{y}_1$ becomes paler and the *personal view* $\mathbf{y}_2$ becomes darker compared to the original images. The parameter r is used to control the trade-off between the *shared view* and *personal view*. A higher value of r results in a better quality of *personal view* but lower quality of the *shared view*. Since the *shared view* $\mathbf{y}_1$ is simply set as the sum of $\mathbf{x}_1$ and $\mathbf{x}_2$, the high spatial frequency areas (i.e., edges) of $\mathbf{x}_2$ may be intrusive. To improve the visual quality of *shared view*, we propose a more sophisticated algorithm in the next section.

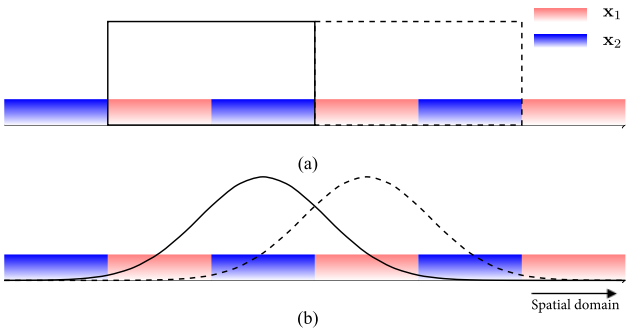

FIGURE 3. Integration windows for the *shared view* in spatial domain. (a) Square integration window, corresponding to the heuristic algorithm. The solid or dashed square means human eyes accumulates two consecutive lines with the same weight. (b) Gaussian integration window, corresponding to the iterative algorithm. The solid or dashed curve means human eyes accumulates several consecutive lines modulated by a Gaussian curve. $\mathbf{x}_1$ and $\mathbf{x}_2$ are the two basis images displayed on odd and even lines, respectively.

III. ITERATIVE ALGORITHM FOR DUAL-VIEW DISPLAY

In the heuristic algorithm, we simply set the odd lines as the personal view and even lines as the difference between the shared view and personal view, which implies that each line of the shared view perceived by the viewer is the sum of the odd line and even line. The solid or dashed square in Fig. 3(a) shows a square integration window that is applied in the heuristic algorithm. Integration window means we summate all the light in the window and the light is weighted by the window. However, human visual systems collect visual information in a spatial area that is not necessary to be exactly only two consecutive lines but over a limited visual field, referred to as spatial integration [16]. The spatial integration extends over 63 deg^2 (circular aperture diameter = 9 deg) in the study of measuring the threshold of discriminating global motion directions [17]. The thresholds decreased as the duration of the area increased. Therefore, the sensitivities of visual systems in the spatial domain decrease from center to the periphery, which can be assumed as a shape of Gaussian curves, shown in Fig. 3(b). The *shared view* will be perceived as the integration of several consecutive lines modulated by a Gaussian curve.

A. FORMULATION OF DUAL-VIEW DISPLAY PROBLEM

The shape of integration windows of visual systems is supposed to be like a Gaussian curve, i.e., increases first and then decreases, and the window is symmetrical with weights summing up to be 1. In practical, the length of the window cannot be infinite like Gaussian curves. Truncated Gaussian-like curves are applied in this paper. The length of window l

(i.e., the number of consecutive basis images in the window) is more than 2 but limited. To formulate the problem, we take $l = 3$ in the spatial domain as an example. Note that the operations below are all in luminance space as discussed in Section II. Thus, the mappings between grayscale space and luminance space are skipped in the following discussion.

The weight for *shared view* can be expressed as $\mathbf{w}_1 = [w_1^1, w_1^0, w_1^1]$, i.e., the spatial integration kernel of human visual systems. It means that every three adjacent lines are weighted by $\mathbf{w}_1$ with step 1. Then we define an auxiliary tridiagonal matrix corresponding to glasses-free viewing

$$\mathbf{A} = \begin{pmatrix} w_1^1 & w_1^0 & w_1^1 & & & \\ & w_1^1 & w_1^0 & w_1^1 & & \\ & & \ddots & \ddots & \ddots & \\ & & & w_1^1 & w_1^0 & w_1^1 \end{pmatrix},$$

and $\mathbf{A}\mathbf{y}_1 = \mathbf{p}_1$, where $\mathbf{A} \in \mathbb{R}^{(H-2)\times H}$, the original *shared view* $\mathbf{y}_1 \in \mathbb{R}^{H\times W}$, and $\mathbf{p}_1 \in \mathbb{R}^{(H-2)\times W}$ is the perceived *shared view*. The goal of our algorithms is to find an image $\mathbf{X} \in \mathbb{R}^{H\times W}$ that displayed on the screen can be perceived as close as possible to $\mathbf{p}_1$. Then the problem can be formulated as

$$\min_{0\le\mathbf{X}\le 1} \frac{1}{2}\|\mathbf{A}\mathbf{y}_1 - \mathbf{A}\mathbf{X}\|_F^2. \tag{4}$$

Certainly, $\mathbf{X} = \mathbf{y}_1$ will be the optimal solution. However, we have another constraint that users with glasses should see a meaningful *personal view*. When with glasses, the even lines of $\mathbf{X}$ are blocked, i.e., $\mathbf{w}_2 = [w_2^1, 0, w_2^1]$. Similarly, we define another auxiliary tridiagonal matrix corresponding to glasses viewing

$$\mathbf{B} = \begin{pmatrix} w_2^1 & 0 & w_2^1 & & & \\ & 0 & 0 & 0 & & \\ & & w_2^1 & 0 & w_2^1 & \\ & & & \ddots & \ddots & \ddots \end{pmatrix},$$

and $\mathbf{B}\mathbf{y}_2 = \mathbf{p}_2$, where $\mathbf{B} \in \mathbb{R}^{(H-2)\times H}$, the original *personal view* $\mathbf{y}_2 \in \mathbb{R}^{H\times W}$, and $\mathbf{p}_2 \in \mathbb{R}^{(H-2)\times W}$ is the perceived *personal view*. Similarly, the display image $\mathbf{X}$ with glasses should be perceived as close as possible to $\mathbf{p}_2$. By adding this constraint, the problem is reformulated as

$$\min_{0\le\mathbf{X}\le 1} \frac{1}{2}\|\mathbf{A}\mathbf{y}_1 - \mathbf{A}\mathbf{X}\|_F^2 + \lambda\frac{1}{2}\|\mathbf{B}\mathbf{y}_2 - \mathbf{B}\mathbf{X}\|_F^2, \tag{5}$$

which can be simplified as

$$\min_{0\le\mathbf{X}\le 1} \frac{1}{2}\|\mathbf{Y} - \mathbf{W}\mathbf{X}\|_F^2, \tag{6}$$

where, $\mathbf{W} = \begin{bmatrix} \mathbf{A} \\ \sqrt{\lambda}\mathbf{B} \end{bmatrix}$ and $\mathbf{Y} = \begin{bmatrix} \mathbf{A}\mathbf{y}_1 \\ \sqrt{\lambda}\mathbf{B}\mathbf{y}_2 \end{bmatrix}$.

B. FACTORIZATION ALGORITHMS

The problem in Eq. (6) is a constrained nonnegative least squares (NNLS) problem. To solve the problem, we use a hierarchical nonnegative least squares (HNNLS) [18] approach, which can boost the convergence rate of the least squares algorithm. In HNNLS, instead of minimizing the cost function directly, the columns of $\mathbf{X}^T$ are updated sequentially. That is, a single column of $\mathbf{X}^T$ is updated while others are fixed. First we define the residues as

$$\mathbf{Y}^{(p)} = \mathbf{Y} - \sum_{j\ne p} \mathbf{W}_{:j}\mathbf{X}_{j:} = \mathbf{Y} - \mathbf{W}\mathbf{X} + \mathbf{W}_{:p}\mathbf{X}_{p:}, \tag{7}$$

where $p = 1, 2, \ldots, H$. The problem in Eq. (6) reduces to a set of cost functions

$$\min_{0\le\mathbf{X}_{p:}\le 1} \frac{1}{2}\|\mathbf{Y} - \mathbf{W}\mathbf{X}\|_F^2 = \frac{1}{2}\|\mathbf{Y}^{(p)} - \mathbf{W}_{:p}\mathbf{X}_{p:}\|_F^2, \tag{8}$$

where $p = 1, 2, \ldots, H$. The gradients of the local cost functions $D_F^{(p)}(\mathbf{Y}^{(p)}\|\mathbf{W}_{:p}\mathbf{X}_{p:})$ in Eq. (8) can be expressed by

$$\frac{\partial D_F^{(p)}(\mathbf{Y}^{(p)}\|\mathbf{W}_{:p}\mathbf{X}_{p:})}{\partial \mathbf{X}_{p:}} = \mathbf{W}_{:p}^T\mathbf{W}_{:p}\mathbf{X}_{p:} - \mathbf{W}_{:p}^T\mathbf{Y}^{(p)}. \tag{9}$$

The sequential learning rules is obtained by equating the gradients to zero and then setting the elements smaller than zero to zero and greater than one to one:

$$\begin{aligned} \mathbf{X}_{p:} &\leftarrow [(\mathbf{W}_{:p}^T\mathbf{W}_{:p})^{-1}\mathbf{W}_{:p}^T\mathbf{Y}^{(p)}]_{[0,1]} \\ &\quad //\text{Replace } \mathbf{Y}^{(p)} \text{ with the Eq. (7).} \\ &= [(\mathbf{W}_{:p}^T\mathbf{W}_{:p})^{-1}\mathbf{W}_{:p}^T(\mathbf{Y} - \mathbf{W}\mathbf{X} + \mathbf{W}_{:p}\mathbf{X}_{p:})]_{[0,1]} \\ &= [(\mathbf{W}_{:p}^T\mathbf{W}_{:p})^{-1}([\mathbf{W}^T\mathbf{Y}]_{p:} - [\mathbf{W}\mathbf{W}^T]_{p:}\mathbf{X} \\ &\qquad + \mathbf{W}_{:p}^T\mathbf{W}_{:p}\mathbf{X}_{p:})]_{[0,1]}. \end{aligned} \tag{10}$$

We denote $\mathbf{C} = \mathbf{W}^T\mathbf{Y}$ and $\mathbf{D} = \mathbf{W}^T\mathbf{W}$. Then the update rule in Eq. (10) can be simplified as

$$\begin{aligned} \mathbf{X}_{p:} &\leftarrow [\frac{\mathbf{C}_{p:} - \mathbf{D}_{p:}\mathbf{X} + \mathbf{D}_{pp}\mathbf{X}_{p:}}{\mathbf{D}_{pp}}]_{[0,1]} \\ &= [\mathbf{X}_{p:} + \frac{\mathbf{C}_{p:} - \mathbf{D}_{p:}\mathbf{X}}{\mathbf{D}_{pp}}]_{[0,1]}. \end{aligned} \tag{11}$$

The pseudocode of the iterative algorithm for the dual-view display is outlined in Algorithm 2.

Algorithm 2 Iterative Algorithm for Dual-View Display

Require: $\mathbf{y}_1, \mathbf{y}_2 \in \mathbb{R}^{H\times W}$, $\mathbf{A}, \mathbf{B} \in \mathbb{R}^{(H-2)\times H}$, $\lambda \ge 0$

Initialize nonnegative matrices $\mathbf{X} \in \mathbb{R}^{H\times W}$;

$\mathbf{W} = \begin{bmatrix} \mathbf{A} \\ \sqrt{\lambda}\mathbf{B} \end{bmatrix}$; $\mathbf{Y} = \begin{bmatrix} \mathbf{A}\mathbf{y}_1 \\ \sqrt{\lambda}\mathbf{B}\mathbf{y}_2 \end{bmatrix}$;

$\mathbf{C} = \mathbf{W}^T\mathbf{Y}$; $\mathbf{D} = \mathbf{W}^T\mathbf{W}$;

repeat

  for $p = 1$ to H **do**

    $\mathbf{X}_{p:} \leftarrow \mathbf{X}_{p:} + \frac{\mathbf{C}_{p:} - \mathbf{D}_{p:}\mathbf{X}}{\mathbf{D}_{pp}}$;

    $\mathbf{X}_{p:} \leftarrow \min(\max(\mathbf{X}_{p:}, \mathbf{0}), \mathbf{1})$;

  end for

until the number of the iterations is reached

return $\mathbf{X} \in \mathbb{R}^{H\times W}$;

IV. EXPERIMENTAL RESULTS AND ANALYSIS

We tested the heuristic algorithm and iterative algorithm in this section. The computer was a Windows 64-bit PC with a 3.4 GHz Intel® Core™ i7-2600K CPU and 16 GB memory. The display monitor was a 23-inch polarized LG display (D2343PB) displaying with a resolution of 1920 × 1080 pixels. The True Color Kodak Images (http://r0k.us/graphics/kodak/) was the image database for simulation.

A. PERFORMANCE METRICS

Peak signal to noise ratio (PSNR) and structural similarity index measure (SSIM) [19] are chosen to be the performance metrics. PSNR measures the similarity between the reconstructed images and the original images and a higher PSNR value indicates a higher image quality. SSIM is a well-known quality metric that is considered to be better correlated with the ratings of human visual systems. Instead of using traditional error summation methods, SSIM is designed by modeling any image distortion as a combination of loss of correlation, luminance distortion, and contrast distortion. In this paper, we further test performance for each component of the objective and define

$$PSNR_{sh} = PSNR(\mathbf{A}\mathbf{y}_1, \mathbf{A}\mathbf{X}), \tag{12}$$
$$PSNR_{ps} = PSNR(\mathbf{B}\mathbf{y}_2, \mathbf{B}\mathbf{X}), \tag{13}$$

and

$$SSIM_{sh} = SSIM(\mathbf{A}\mathbf{y}_1, \mathbf{A}\mathbf{X}), \tag{14}$$
$$SSIM_{ps} = SSIM(\mathbf{B}\mathbf{y}_1, \mathbf{B}\mathbf{X}). \tag{15}$$

B. PARAMETER SELECTION

There are five parameters explicit and implicit in the dual-view display problem Eq. (6): λ, r_1, r_2, σ, and l. λ is a regularization coefficient to trade off the qualities between the *shared view* and *personal view*. Apparently, a larger λ results in a higher quality of *personal view* and lower quality of *shared view*. In this paper, we choose $\lambda = 1$ and it can be adjusted according to the requirements in a real situation. r_1 and r_2 are used to adjust the luminance range of *shared view* and *personal view*, respectively. The luminance range of *shared view* or *personal view* increases as r_1 or r_2 increases. σ is used to control the weights in the integration window between the center and periphery. A larger σ represents a higher weight in the center area. l is the truncated window length for $\mathbf{w}_1$ and $\mathbf{w}_2$.

1) LUMINANCE RANGES r_1, r_2

Although, the iterative algorithm will not result in out of the $[0, 1]$ range for the output images, properly adjusting the luminance ranges can improve the qualities of *shared view* and *personal view* significantly. The results of adjusting r_1 are shown in TABLE 2. As r_1 increases, *PSNR*s and *SSIM*s decrease. That is, when the range of *shared view* increases, the image similarity with the original one decreases slightly. However, high luminance range can improve the visual quality subjectively. Considering the trade-off between image similarity and luminance range, we choose $r_1 = 0.8$ (i.e., $\mathbf{y}_1 \in [0.2, 1]$). Similarly, the results of adjusting r_2 are presented in TABLE 3. As r_2 increases, $PSNR_{sh}$, $PSNR_{ps}$, and $SSIM_{sh}$ decrease, but $SSIM_{ps}$ is nearly constant. Therefore, we choose $r_2 = 0.8$ (i.e., $\mathbf{y}_2 \in [0, 0.8]$) to balance the luminance range and image similarity.

TABLE 2. ***PSNR*** **and** ***SSIM*** **for different values of r_1 when $\lambda = 1$, $r_2 = 0.8$, $l = 3$, $\sigma = 0.5$.**

$r_1 =$	0.6	0.65	0.7	0.75	0.8	0.85	0.9	0.95
$PSNR_{sh}$	**42.6**	42.4	42.2	41.9	41.5	40.8	39.5	37.1
$PSNR_{ps}$	**45.0**	44.9	44.7	44.4	44.1	43.5	42.2	39.8
$SSIM_{sh}(\%)$	**96.7**	96.7	96.7	96.7	96.7	96.6	96.2	95.5
$SSIM_{ps}(\%)$	**99.8**	99.8	99.8	99.7	99.7	99.7	99.7	99.5

TABLE 3. ***PSNR*** **and** ***SSIM*** **for different values of r_2 when $\lambda = 1$, $r_1 = 0.8$, $l = 3$, $\sigma = 0.5$.**

$r_2 =$	0.6	0.65	0.7	0.75	0.8	0.85	0.9	0.95
$PSNR_{sh}$	**43.2**	42.8	42.4	41.9	41.5	41.0	40.5	40.0
$PSNR_{ps}$	**46.2**	45.6	45.1	44.6	44.1	43.6	43.0	42.5
$SSIM_{sh}(\%)$	**97.9**	97.6	97.3	97.0	96.7	96.3	95.9	95.5
$SSIM_{ps}(\%)$	99.7	99.7	99.7	99.7	99.7	99.7	99.7	99.7

2) CENTER WEIGHT σ

Suppose the length of window is $l = 3$, the parameter σ means $\mathbf{w}_1 = [(1-\sigma)/2, \sigma, (1-\sigma)/2]$, i.e., the weight of the window's center area. The results are shown in Fig. 4 and TABLE 4. As σ increases, the *PSNR*s and *SSIM*s increase first and then decrease. They are at the maximums when $\sigma = 0.5$, indicating that the two basis images $\mathbf{x}_1$ and $\mathbf{x}_2$ should have the same weights totally in the integration window.

TABLE 4. ***PSNR*** **and** ***SSIM*** **for different values of σ when $\lambda = 1$, $r_1 = 0.8$, $r_2 = 0.8$, and $l = 3$.**

$\sigma =$	0.35	0.4	0.45	0.5	0.55	0.6	0.65	0.7
$PSNR_{sh}$	19.1	21.8	27.1	**41.5**	26.9	21.7	19.1	17.6
$PSNR_{ps}$	26.9	32.8	41.9	**44.1**	39.7	31.9	26.5	23.0
$SSIM_{sh}(\%)$	26.0	33.8	54.3	**96.7**	53.8	34.0	26.7	23.7
$SSIM_{ps}(\%)$	81.2	90.2	98.2	**99.7**	97.8	89.5	80.5	72.9

3) WINDOW LENGTH l

The larger window length, the more spatial lines are covered by the window. In our experiments, we choose the length l from 3 to 8. With the guidance of σ, we set the weights of windows as shown in TABLE 5. The weights are tuned to achieve the best performance. The results are presented in TABLE 6. When l increases, the *PSNR*s and *SSIM*s increase as well. However, the improvements are slight when $l > 4$.

Here, we evaluate the computational time of the heuristic and iterative algorithm. Figure 5 presents the time complexity result. The parameters for iterative algorithm were $\lambda = 1$, $r_1 = 0.8$, $r_2 = 0.8$, $\sigma = 0.5$, and $l = 5$. The parameter for

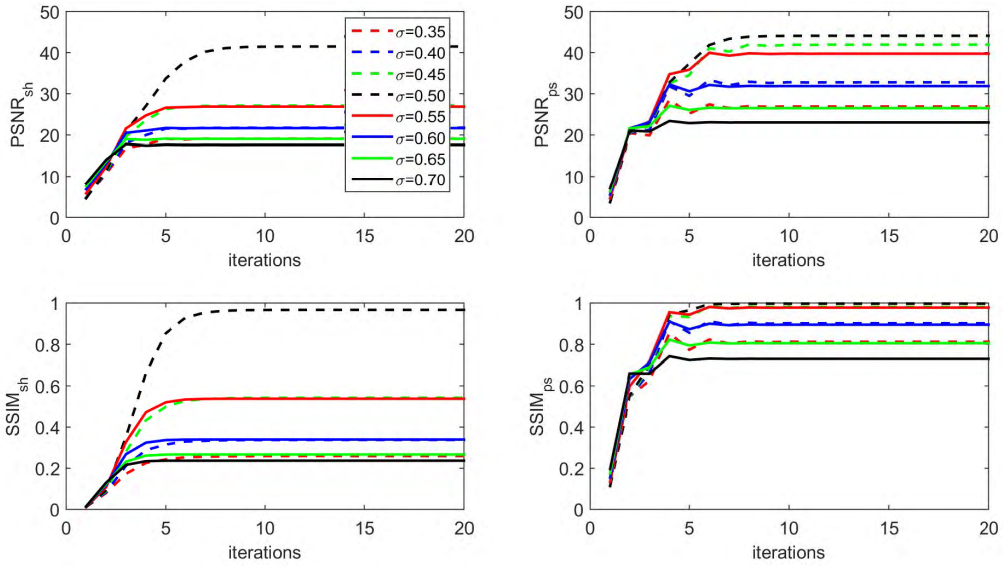

FIGURE 4. *PSNR* and *SSIM* versus iterations for different values of σ when $\lambda = 1$, $r_1 = 0.8$, $r_2 = 0.8$, and $l = 3$.

TABLE 5. Spatial integration windows for different window length l.

l	$\mathbf{w}_1$	$\mathbf{w}_2$
3	0.25, 0.5, 0.25	0.5, 0, 0.5
4	0.15, 0.35, 0.35, 0.15	0, 0.5, 0, 0.5
5	0.05, 0.25, 0.4, 0.25, 0.05	0.25, 0, 0.5, 0, 0.25
6	0.02, 0.14, 0.34, 0.34, 0.14, 0.02	0, 0.25, 0, 0.5, 0, 0.25
7	0.01, 0.05, 0.24, 0.40, 0.24, 0.05, 0.01	0.15, 0, 0.35, 0, 0.35, 0, 0.15
8	0.03, 0.05, 0.12, 0.3, 0.3, 0.12, 0.05, 0.03	0, 0.15, 0, 0.35, 0, 0.35, 0, 0.15

TABLE 6. *PSNR* and *SSIM* for different values of l when $\lambda = 1$, $r_1 = 0.8$, $r_2 = 0.8$, and $\sigma = 0.5$.

$l =$	3	4	5	6	7	8
$PSNR_{sh}$	41.5	46.4	47.5	47.6	47 8	**48.3**
$PSNR_{ps}$	44.1	50.0	50.5	51.0	51.5	**51.7**
$SSIM_{sh}(\%)$	96.7	99.0	99.2	99.2	99.2	**99.4**
$SSIM_{ps}(\%)$	99.7	99.9	99.9	1	1	**1**

heuristic algorithm was $r = 0.25$. Each algorithm was tested for 100 times. The computational time is 0.2914 ± 0.0116 seconds for heuristic algorithm and 2.8668 ± 0.1581 seconds for iterative algorithm after 18 iterations (9 iterations are close enough as shown in Fig. 4). Note that, we can reduce the computational time using C++ or other hardware platforms like GPUs, FPGAs, and TPUs.

C. SUBJECTIVE EXPERIMENT

In this subsection, we set up a subjective experiment to test the performances of the heuristic algorithm and iterative algorithm for the *shared view* and *personal view*. We chose 12 images with a resolution of 768×512 from the True Color Kodak Images. Every two images can be a pair of the *shared view* and *personal view*. Totally, there are $A_{12}^2 = 12 \times 11 = 132$ combinations. For each combination, the views generated

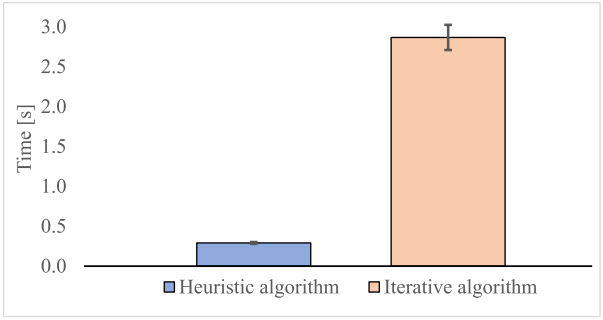

FIGURE 5. Time complexity comparison between the heuristic and iterative algorithm using Matlab. Each algorithm was tested for 100 times. The computational time is 0.2914 ± 0.0116 seconds for heuristic algorithm and 2.8668 ± 0.1581 seconds for iterative algorithm.

by the heuristic and iterative algorithm are presented on the screen side by side randomly, as shown in Fig. 6.

Eleven subjects with the ages from 23 to 27 were recruited for this study. The subjects sat right ahead of the 23-inch polarized LG 3D display at a distance of 0.5 meter. We required the subjects to make forced-choices to decide which side of the views is better. The experiment included two trials. In the first trial, subjects viewed the display without the glasses, i.e., the test for *shared view*. In the second trial, subjects viewed the display with the glasses, i.e., the test for

TABLE 7. Results of the subjective experiment. HA and IA represent the heuristic algorithm and iterative algorithm, respectively. IA(%) is the percentage where the images generated by the iterative algorithm are better than that by the heuristic algorithm. On average, the *shared views* and *personal views* generated by the iterative algorithm are better than the heuristic algorithm with the percentages of 90.2% and 64.9%, respectively.

Subject		1	2	3	4	5	6	7	8	9	10	11	AVE
Shared view	HA	31	11	9	10	9	17	19	18	8	5	5	13
	IA	101	121	123	122	123	115	113	114	124	127	127	119
	IA(%)	76.5	91.7	93.2	92.4	93.2	87.1	85.6	86.4	93.9	96.2	96.2	**90.2**
Personal view	HA	43	37	90	85	61	74	5	7	59	42	7	46
	IA	89	95	42	47	71	58	127	125	73	90	125	86
	IA(%)	67.4	72.0	31.8	35.6	53.8	43.9	96.2	94.7	55.3	68.2	94.7	**64.9**

FIGURE 6. The views by the heuristic and iterative algorithms are presented side by side at the same time. The *shared view* and *personal view* can be seen with or without the glasses.

personal view. TABLE 7 shows the results of the subjective experiment. The parameters for the iterative algorithm were $\lambda = 1$, $r_1 = 0.75$, $r_2 = 0.75$, $\sigma = 0.5$, and $l = 5$. The parameter for the heuristic algorithm was $r = 0.25$. Here we change the dynamic ranges r_1 and r_2 from 0.8 to 0.75 to make sure the *shared views* generated by the two algorithms have the same dynamic range. Pairwise t-tests were performed on *shared views* and *personal views* (between the iterative and heuristic algorithm), as shown in Fig. 7. The images generated by these two algorithms are presented in Fig. 8 and 9. The images were captured by Sony NEX-VG20E, which was used for simulating the views of human eyes. Note that, the integral kernels of human eyes and digital camera are not exactly the same. We adjust the parameters in the camera to make the simulations close to the visual results.

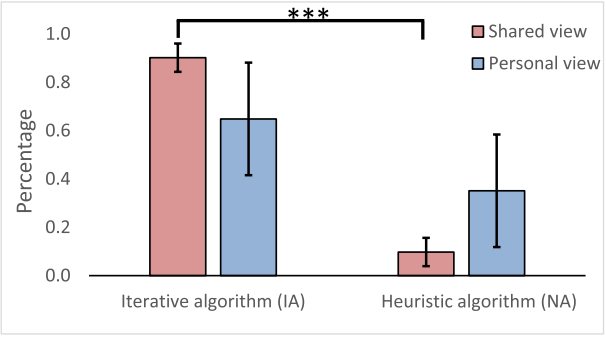

FIGURE 7. Results of the subjective experiment. The iterative algorithm performed significantly better than the heuristic algorithm ($t(10) = 22.75, p < 0.001$).

For *shared view*, the iterative algorithm performs significantly better than the heuristic algorithm ($t(10) = 22.75$, $p < 0.001$), as shown in Fig. 7. The percentage that the *shared views* generated by the iterative algorithm were better than the heuristic algorithm is 90.2% on average. The *shared views* generated by the heuristic algorithm contain some artifacts of edge contours from the *personal view*, as shown in the red rectangles in Fig. 8(a), 8(c) and Fig. 9(a), 9(c). The iterative algorithm eliminates these artifacts and improves the quality of *shared view* greatly.

For *personal view*, we found no significant improvement between the iterative algorithm and the heuristic algorithm ($t(10) = 2.12, p = 0.06$), as shown in Fig. 7. On average, the *personal views* generated by the iterative algorithm are better than that by the heuristic algorithm with a percentage of 64.9%. The standard deviation of the results is 23.3%. This is because different people have different preferences. The iterative algorithm can lead to higher dynamic range compared to the heuristic algorithm (Fig. 9(b)), but also will introduce relatively small artifacts, as shown in the red rectangles in Fig. 8(b), 8(d) and Fig. 9(b), 9(d). For subjects 3 and 4, they were sensible to the artifacts and preferred the lower dynamic range views. For subjects 7, 8, and 11, they were not bothered by the artifacts and preferred the higher dynamic range views. The others balanced the pros and cons of each algorithm for different views.

V. DISCUSSION

High resolution of modern displays can offer much more information than what human visual systems can resolve. Because the discrimination capacity of human eyes is limited, the neighboring pixels in the spatial domain will be fused as a single one. Therefore, theoretically, modern displays with high resolution can be explored to achieve multi-view display based on SPVM.

At the present stage, the commercially available stereoscopic 3D displays can only achieve dual-view display. Several applications [14], [15] has been implemented based on the dual-view display using the heuristic algorithm. The heuristic algorithm are simple and can be implemented in real time using C++ [7], [14]. However, the *shared views* contain some edge contours leaking from the *personal view* (shown in Fig. 8), which reduces the visual quality greatly. Thus, we proposed a new iterative algorithm to improve the performance of the dual-view display.

The iterative algorithm is based on the characteristic of the spatial integration window in human visual systems. We formulate mathematical models to simulate the integration processes, as shown in Eq. (6). Compared to the heuristic

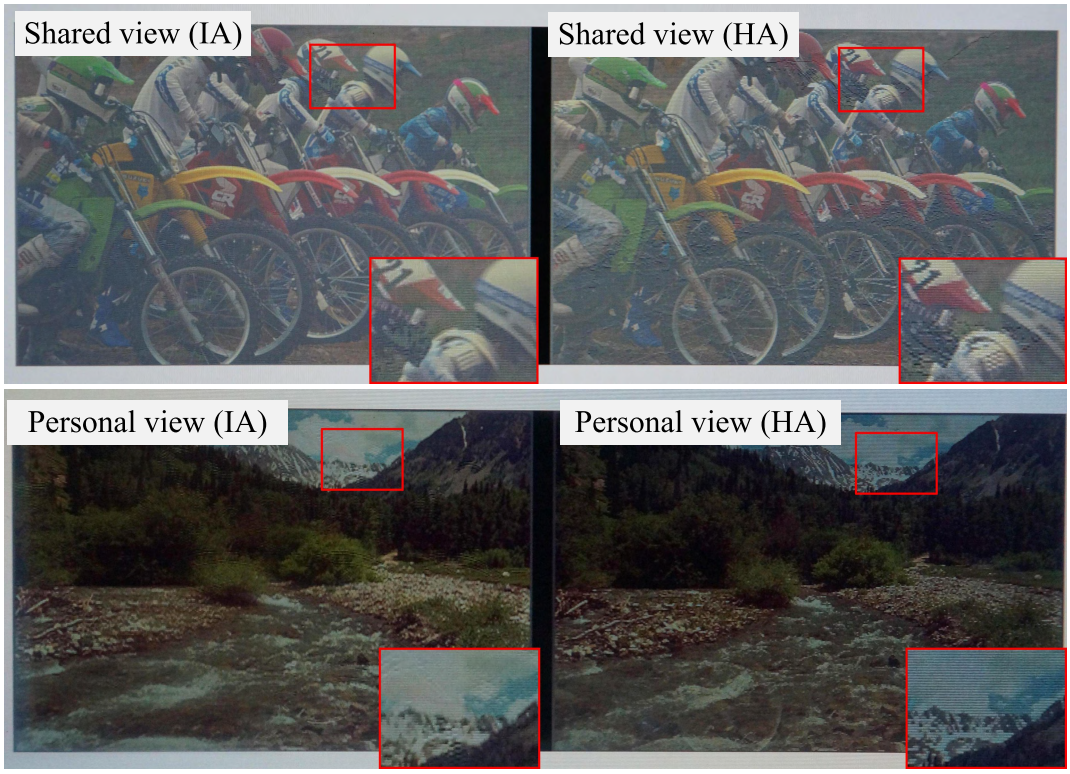

(a)

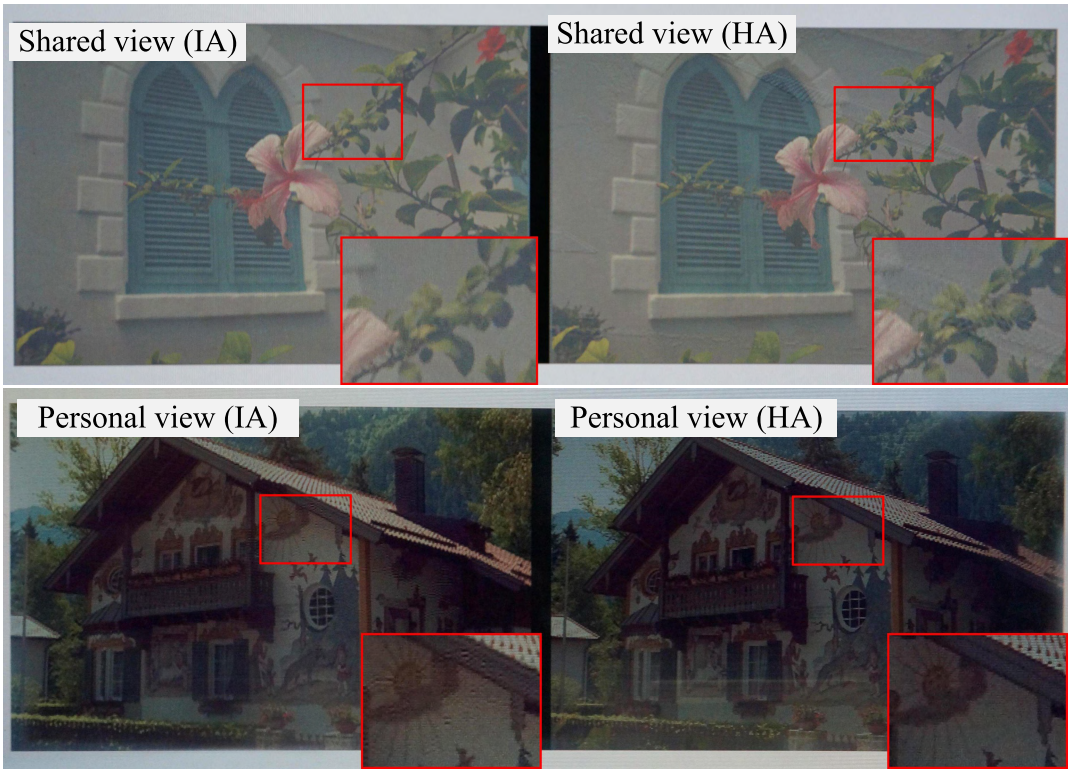

(b)

FIGURE 8. Two pairs of results for the *shared view* and *personal view* in the dual-view display. Left and right images are the results of the iterative algorithm (IA) and heuristic algorithm (HA) respectively. These images are captured by Sony NEX-VG20E, which is used for simulating the views of human eyes. (a) pair one. (b) pair two.

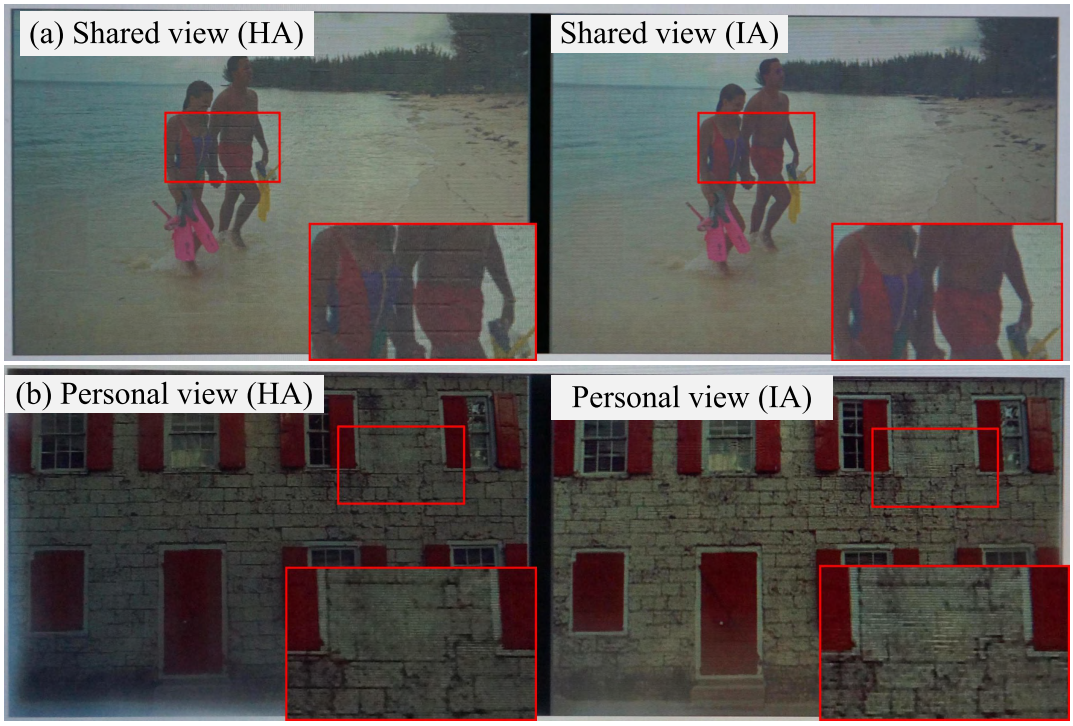

(a)

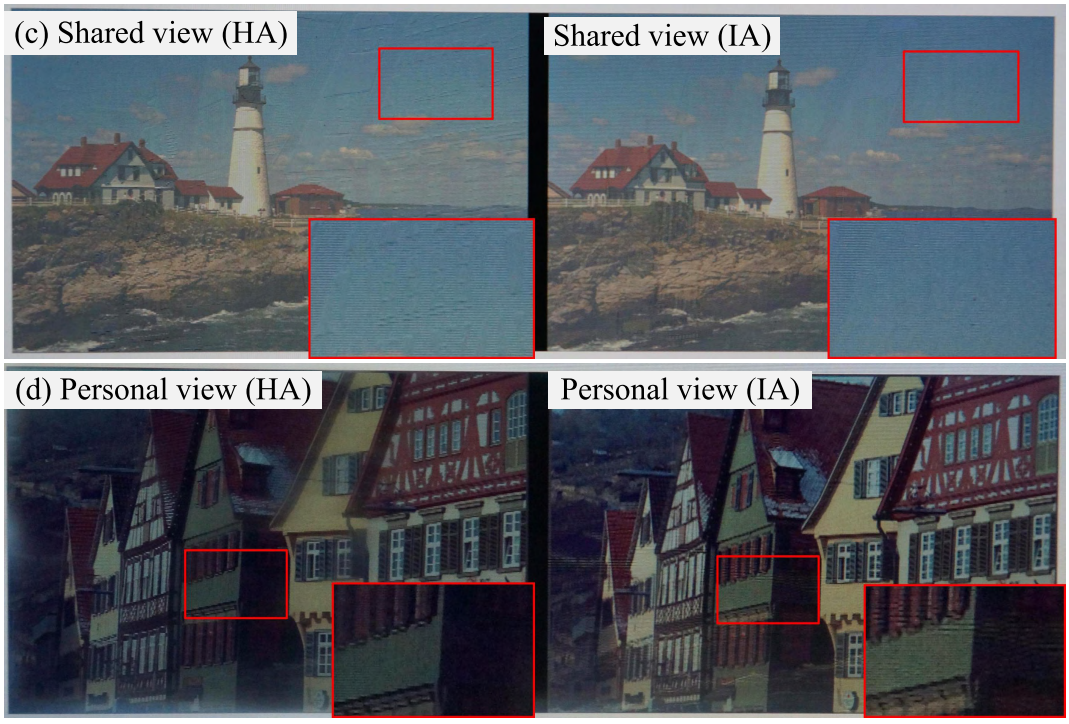

(b)

FIGURE 9. Two pairs of results for the *shared view* and *personal view* in the dual-view display. Left and right images are the results of the heuristic algorithm (HA) and iterative algorithm (IA) respectively. These images are captured by Sony NEX-VG20E, which is used for simulating the views of human eyes. (a) pair one. (b) pair two.

algorithm, the iterative algorithm can remove edge contours leaking from the *personal view* and improve the *shared view* greatly. Moreover, the dynamic range of *personal view* using iterative algorithm is higher than using heuristic algorithm. For heuristic algorithm, the dynamic range of *personal view* is constricted to $[0, r]$ when the range of *shared view* is set to $[r, 1]$, i.e., the sum of the ranges is 1. However, for iterative algorithm, the dynamic ranges of *personal view* and

shared view are initialized to $[0, r_2]$ and $[1 - r_1, 1]$, and then are adjusted by the algorithm automatically. The sum of the initial ranges can be larger than 1 (i.e., $r_1 + r_2 > 1$ is feasible). Iterative algorithm has one shortcoming. The heuristic algorithm presents the *personal view* on even lines directly after range adjustment while the iterative algorithm will alter contour areas of the *personal view* to improve the image quality of *shared view*, which may introduce some artifacts to the *personal view*. However, the introduced artifacts are relatively small since they are usually at around edge contours. Moreover, the *personal view* is darker than the *shared view* since the *personal view* needs to be seen through a pair of glasses and is at a lower dynamic range (i.e., $[0, r_2]$ compared to $[1-r_1, 1]$), making the artifacts more imperceptible.

Note that, the spatial integration window of human eyes is defined in angular [17]. Thus, the integration window depends both on the screen pixel density (in PPI) and the viewing distance. On the 23-inch 3D display used in our experiment, we used the effective integration window that covers 5 lines at 0.5m viewing distance, which is 9.6 arcmins. When the viewing distance for the 23-inch 3D display is between 0.3m and 0.8m (i.e., a recommended viewing distance range with the field of view between 80° and 35°), the same effective integration window covers 3 lines and 8 lines for the 0.3m and 0.8m viewing distance, respectively. As analyzed in Section IV.B, the iterative algorithm with 3-line window length performances well and a larger window length can achieve better. It could reasonably be inferred that the image quality would not degrade too much at a close but normal viewing distance. A further viewing distances performances better but results in smaller visual fields. Importantly, a higher screen pixel density can improve the image quality greatly.

This paper only focuses on the spatial domain of the dual-view display system. In temporal domain, some applications have also been implemented. An information security display system was introduced in [7]. A simultaneous triple subtitles exhibition system was designed in [20]. A 3D/2D concurrent viewing system was introduced in [21] and [22] that viewers wearing 3D glasses perceive a stereoscopic image and viewers without 3D glasses can perceive a conventional 2D image without ghost artifacts. The mathematical model for the spatial domain can also be applied to the temporal domain. Further experiments in the temporal domain will be studied in the future.

VI. CONCLUSION

In this paper, we introduce a dual-view display technology on polarized 3D displays, where users with specific glasses can see one view and without the glasses see another view. This is because modern displays have high resolution so that they can provide more information than human visual systems can resolve. Spatial psychovisual modulation (SPVM) that has the ability to explore the redundancies of modern displays in the spatial domain is used to achieve the dual-view display. We summarize the heuristic algorithm for the dual-view display and propose an iterative algorithm to improve the performance of the system based on the shape of spatial integration of human eyes. The improvements are conspicuous for the *shared view* ($t(10) = 22.75, p < 0.001$). Dual-view or multi-view display combining temporal redundancy of modern displays will be studied in the future.

REFERENCES

[1] S. Pastoor and M. Wöpking, "3-D displays: A review of current technologies," *Displays*, vol. 17, no. 2, pp. 100–110, Apr. 1997. [Online]. Available: http://www.sciencedirect.com/science/article/pii/S0141938296010402

[2] F. F. Kuhlman, A. P. Harbach, R. D. Parker, and D. H. R. Sarma, "Dual view display system using a transparent display," U.S. Patent 8 362 992, Jan. 29, 2013.

[3] J.-P. Cui, Y. Li, J. Yan, H.-C. Cheng, and Q.-H. Wang, "Time-multiplexed dual-view display using a blue phase liquid crystal," *J. Display Technol.*, vol. 9, no. 2, pp. 87–90, Feb. 2013.

[4] F. Wu, H. Deng, C.-G. Luo, D.-H. Li, and Q.-H. Wang, "Dual-view integral imaging three-dimensional display," *Appl. Opt.*, vol. 52, no. 20, pp. 4911–4914, Jul. 2013. [Online]. Available: http://ao.osa.org/abstract.cfm?URI=ao-52-20-4911

[5] C. P. Chen, J. H. Lee, T.-H. Yoon, and J. C. Kim, "Monoview/dual-view switchable liquid crystal display," *Opt. Lett.*, vol. 34, no. 14, pp. 2222–2224, Jul. 2009. [Online]. Available: http://ol.osa.org/abstract.cfm?URI=ol-34-14-2222

[6] C.-T. Hsieh, J.-N. Shu, H.-T. Chen, C.-Y. Huang, C.-J. Tian, and C.-H. Lin, "Dual-view liquid crystal display fabricated by patterned electrodes," *Opt. Express*, vol. 20, no. 8, pp. 8641–8648, Apr. 2012. [Online]. Available: http://www.opticsexpress.org/abstract.cfm?URI=oe-20-8-8641

[7] Z. Gao, G. Zhai, and X. Min, "Information security display system based on temporal psychovisual modulation," in *Proc. IEEE Int. Symp. Circuits Syst. (ISCAS)*, Jun. 2014, pp. 449–452.

[8] X. Wu and G. Zhai, "Temporal psychovisual modulation: A new paradigm of information display [exploratory DSP]," *IEEE Signal Process. Mag.*, vol. 30, no. 1, pp. 136–141, Jan. 2013.

[9] J. Liu, S.-M. Morgens, R. C. Sumner, L. Buschmann, Y. Zhang, and J. Davis, "When does the hidden butterfly not flicker?" in *Proc. SIGGRAPH Asia Tech. Briefs (SA)*. New York, NY, USA: ACM, 2014, Art. no. 3, doi: 10.1145/2669024.2669026.

[10] Texas Instruments. (2016). *DLP Discovery 4100 Development Kit*. [Online]. Available: http://www.ti.com/tool/dlpd4x00kit

[11] Pixensity. (2016). *Phone Pixel Density (PPI) List*. [Online]. Available: http://pixensity.com/list/phone/

[12] D. H. Kelly, "Visual contrast sensitivity," *Optica Acta, Int. J. Opt.*, vol. 24, no. 2, pp. 107–129, 1977, doi: 10.1080/713819495.

[13] Y. Takubo, Y. Hisatake, T. Lizuka, and T. Kawamura, "64.1: *Invited paper*: Ultra-high resolution mobile displays," in *SID Symp. Dig. Tech. Papers*, 2012, vol. 43, no. 1, pp. 869–872, doi: 10.1002/j.2168-0159.2012.tb05924.x.

[14] C. Hu, G. Zhai, Z. Gao, and X. Min, "Information security display system based on spatial psychovisual modulation," in *Proc. IEEE Int. Conf. Multimedia Expo (ICME)*, Jul. 2014, pp. 1–4.

[15] Z. Gao, G. Zhai, C. Hu, and X. Min, "Dual-view medical image visualization based on spatial-temporal psychovisual modulation," in *Proc. 21st IEEE Int. Conf. Image Process. (ICIP)*, Oct. 2014, pp. 2168–2170.

[16] R. E. Näsänen, H. T. Kukkonen, and J. M. Rovamo, "A window model for spatial integration in human pattern discrimination," *Invest. Ophthalmol. Vis. Sci.*, vol. 36, no. 9, pp. 1855–1862, 1995.

[17] S. N. J. Watamaniuk and R. Sekuler, "Temporal and spatial integration in dynamic random-dot stimuli," *Vis. Res.*, vol. 32, no. 12, pp. 2341–2347, 1992.

[18] A. Cichocki and A.-H. Phan, "Fast local algorithms for large scale nonnegative matrix and tensor factorizations," *IEICE Trans. Fundam. Electron., Commun. Comput. Sci.*, vol. E92-A, no. 3, pp. 708–721, 2009.

[19] Z. Wang, A. C. Bovik, H. R. Sheikh, and E. P. Simoncelli, "Image quality assessment: From error visibility to structural similarity," *IEEE Trans. Image Process.*, vol. 13, no. 4, pp. 600–612, Apr. 2004.

[20] C. Hu, G. Zhai, Z. Gao, and X. Min, "Simultaneous triple subtitles exhibition via temporal psychovisual modulation," in *Proc. 9th IEEE Conf. Ind. Electron. Appl.*, Jun. 2014, pp. 944–947.

[21] X. Wu and G. Zhai, "Backward compatible stereoscopic displays via temporal psychovisual modulation," in *Proc. SIGGRAPH Asia Emerg. Technol. (SA)*. New York, NY, USA: ACM, 2012, Art. no. 4, doi: 10.1145/2407707.2407711.
[22] S. Scher, J. Liu, R. Vaish, P. Gunawardane, and J. Davis, "3D+2DTV: 3D displays with no ghosting for viewers without glasses," *ACM Trans. Graph.*, vol. 32, no. 3, Jul. 2013, Art. no. 21, doi: 10.1145/2487228.2487229.

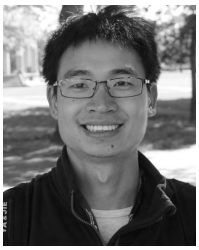

ZHONGPAI GAO received the B.Sc. degree in electronic and information engineering from the Huazhong University of Science and Technology, Wuhan, China, in 2013. He is currently pursuing the Ph.D. degree in electrical engineering with Shanghai Jiao Tong University, Shanghai, China. He was a Visiting Ph.D. Student with the Schepens Eye Research Institute, Harvard Medical School, Boston, USA, from 2016 to 2018. His research interests include multimedia signal processing, stereoscopic 3-D, visually induced motion sickness, and psychovisual modulation display technology.

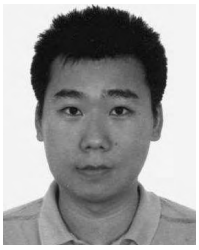

GUANGTAO ZHAI (M'10) received the B.E. and M.E. degrees from Shandong University, Jinan, China, in 2001 and 2004, respectively, and the Ph.D. degree from Shanghai Jiao Tong University, Shanghai, China, in 2009. He is currently a Research Professor with the Institute of Image Communication and Network Engineering, Shanghai Jiao Tong University.

He was a Student Intern with the Institute for Infocomm Research, Singapore, from 2006 to 2007. He was a Visiting Student with the School of Computer Engineering, Nanyang Technological University, Singapore, from 2007 to 2008, and with the Department of Electrical and Computer Engineering, McMaster University, Hamilton, ON, Canada, from 2008 to 2009, where he was also a Post-Doctoral Fellow from 2010 to 2012. From 2012 to 2013, he was a Humboldt Research Fellow with the Institute of Multimedia Communication and Signal Processing, Friedrich Alexander University of Erlangen-Nuremberg, Erlangen, Germany. His research interests include multimedia signal processing and perceptual signal processing. He was a recipient of the National Excellent Ph.D. Thesis Award from the Ministry of Education of China in 2012.